International Journal of Heat and Mass Transfer 131 (2019) 150–166

Contents lists available at ScienceDirect

International Journal of Heat and Mass Transfer

journal homepage: www.elsevier.com/locate/ijhmt

Inverse heat transfer method applied to capacitively cooled rocket thrust chambers

Nikolaos Perakis *, Oskar J. Haidn

Technical University of Munich, Chair of Turbomachinery and Flight Propulsion, Boltzmannstr. 15, 85748 Garching, Germany

ARTICLE INFO

Article history:
Received 9 August 2018
Received in revised form 16 October 2018
Accepted 9 November 2018

Keywords:
Inverse method
Rocket engine
Methane combustion
Heat transfer

ABSTRACT

Measurements of the heat loads in experimental lab-scale rocket combustors are essential in order to obtain information about the mixing and energy release of the propellants, the injector/injector interaction as well as the injector/wall interaction. Usually the hardware used for single-element rocket thrust chambers is capacitively cooled in order to reduce the complexity of the system. The present work demonstrates an efficient method for estimating the time- and spatially resolved heat flux distribution at the hot gas wall of such engines using the information provided by temperature measurements in the material. The method is implemented in the code RoqFITT (Rocket $\dot{q}$ Flux Inverse Thermal Tool) and is applied for the evaluation of test data of CH_4/O_2 and H_2/O_2 experiments. Three separate capacitive combustors are investigated, which are operated at the Chair of Turbomachinery and Flight Propulsion (LTF) of the Technical University of Munich (TUM): a single-element cylindrical, a single-element rectangular and a multi-element rectangular chamber. The use of the 3D inverse method for different load points gives significant information about the effect of the different propellant combinations, the choice of mixture ratio and pressure level, the spanwise heat flux distribution and hence injector/injector interaction as well as the transient effects during the igniter operation.

1. Introduction

The development process of new hardware and introduction of new technologies for rocket engines usually requires the design and testing of sub-scale engines. Specifically, before the design of full-scale engines, tests using single-element and multi-element sub-scale hardware are performed [1–4]. The knowledge about the performance of the injector elements, i.e. the mixing of the propellants, the injector/injector interaction and injector/wall interaction in the sub-scale experiments is used as an input for the improvement of the full-scale design without the need for costly full-scale testing.

Sub-scale configurations using single-element and multi-element rocket combustors are also used to provide validation data for numerical simulations. Over the past decades, significant effort has been placed in the numerical calculation of the combustion process in rocket engines. The necessity for a reliable prediction of the combustion characteristics and the heat loads within a combustion chamber and nozzle has promoted computational fluid dynamics (CFD) to become an integral part of the design process in the space propulsion industry. The validation of these numerical tools is usually done by comparing the calculated results for performance (Isp, c^*), pressure profiles along the axial position $p_c(x)$ as well as the heat flux values at the hot gas wall $\dot{q}(x)$ to the available experimental data. This implies that trustworthy measurements with sufficient axial resolution for those values have to be available by the experiments over a wide range of operational conditions. The need for this data is even more critical for the innovative propellant combination of methane (CH_4) and oxygen (O_2) due to the limited number of available tests [5–9].

Of the previously mentioned quantities, the one having the largest significance for the understanding of the physical and chemical phenomena is the heat flux. Due to the harsh environment within the chamber hot gas, the installation of sensors measuring temperature is almost impossible. Therefore, access to the burning gas is very limited and direct measurement is quite challenging and usually restricted to optical measurements of radicals emission or to spectroscopic methods like the Coherent anti-Stokes Raman (CARS) spectroscopy [10]. These methods however require the active film cooling of the optical window which can lead to a distortion of the flow field. Specifically, in single injector combustion chambers with strong film cooling the acceleration distribution due to hot gas expansion by combustion is not always

* Corresponding author.
E-mail address: nikolaos.perakis@tum.de (N. Perakis).

https://doi.org/10.1016/j.ijheatmasstransfer.2018.11.048
0017-9310/

representative due to the interaction with the film. Due to these difficulties, the heat flux distributions are usually utilized to deduce information about the conditions within the chamber.

Moreover the prediction of the engines lifetime, the design of an effective cooling system and the reliability of the chamber components after a specific number of tests is imminently connected to the heat loads applied onto the chamber wall thereby increasing the importance of this value even more.

The calculation of the heat flux in experiments where no active cooling system is present becomes challenging since the only information available consists of temperature readings at specific locations in the chamber material. The reconstruction of the heat flux profiles requires the solution of an inverse problem. The problem is considered to be an "inverse" one, since the causes (heat flux) that lead to a measured effect (temperature at specific locations) are sought.

The present work gives an overview of the capabilities of the inverse heat conduction method when applied to single- and multi-element chambers and the information about the flowfield and heat release that can be deduced from the resulting heat flux values. The hardware examined is operated at the Chair of Turbomachinery and Flight Propulsion (LTF) of the Technical University of Munich (TUM). Test data from experiments using gaseous methane (GCH_4) and gaseous oxygen (GO_2) as propellants as well as gaseous hydrogen (GH_2) and GO_2 are used for the validation of the method.

2. Inverse heat conduction method

Experimental lab-scale rocket combustors cooled by a water cycle or other cooling medium have the characteristic property of reaching a steady state temperature distribution after the first seconds of operation. This effect can be utilized when evaluating the heat flux profiles, since the latter ones can simply be obtained from the enthalpy difference of the outgoing and incoming coolant flow. When dealing with capacitively cooled engines however, the temperature field is not stationary during the test operation and hence a transient inverse heat conduction method is needed. Several efforts have been performed to calculate the transient heat flux profiles [11,12] in generic configurations as well as explicitely in rocket engines [13,14].

The main concept behind an inverse method for heat conduction problems lies in trying to estimate the boundary conditions (causes) which best fit the measured temperature values (effects) while keeping the physics of the problem intact. Similarly to the majority of inverse algorithms, the method shown in the present work is based on an iterative approach as outlined in Fig. 1. The goal of the optimization is to minimize the difference between the measured and calculated temperatures at the measurement locations.

The starting point of the code is to initialize the temperature in the computational domain and to choose an initial guess for the heat flux. With the initial conditions (temperature field) and the boundary conditions (guessed heat flux) the first step is solving the direct heat conduction problem. A restriction for the capacitively cooled chamber is that the starting point for the evaluation is always the beginning of the test. The reason is that the initial conditions in the entire domain have to be exactly known in order to initiate the calculation. The only time point where a known temperature field is present in the entire domain is at $t = 0$s, when the structural material is still at ambient temperature.

2.1. Direct solver

For the solution of the direct problem, a direct solver is required, which has to be computationally very efficient. This is a strict requirement due to the large number of direct problem evaluations until convergence of the heat flux is achieved. For the solution of the thermal conduction problem, RoqFITT uses a 3D finite difference (FD) code which was developed specifically for this purpose by the authors and has been validated in Celano et al. [15] and Perakis et al. [16]. The implementation of the direct solver is carried out in Matlab to avoid any extra interfaces between the optimization code and the direct solver. A central difference approximation of the second derivative in the heat conduction equation (Eq. (1)) is combined with an implicit Euler scheme for the time integration.

$$\frac{\partial T}{\partial t} = \frac{\lambda}{\rho c_p} \nabla^2 T \tag{1}$$

The FD solver is used to solve the heat conduction partial differential equation (PDE) in a simplified geometry. The geometry consists only of the copper combustion chamber (excluding the nozzle segment) and is in principle a block with a hole in the middle at the location where the hot gas combustion takes place. The exclusion of the nozzle is due to the fact that no temperature data are available in the nozzle block. As shown in Section 3 all of the combustors have a very short nozzle since the focus of the experiment is in understanding the combustion processes in the chamber and not to obtain high specific impulse and thrust performance. Eq. (1) is solved in Cartesian coordinates for the rectangular chambers and in cylindrical ones for the cylindrical hardware. The simplified

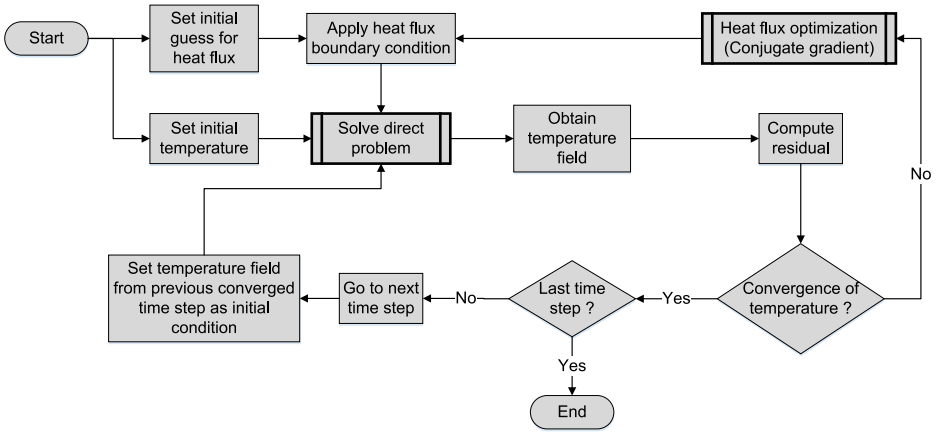

Fig. 1. Inverse heat conduction iterative algorithm.

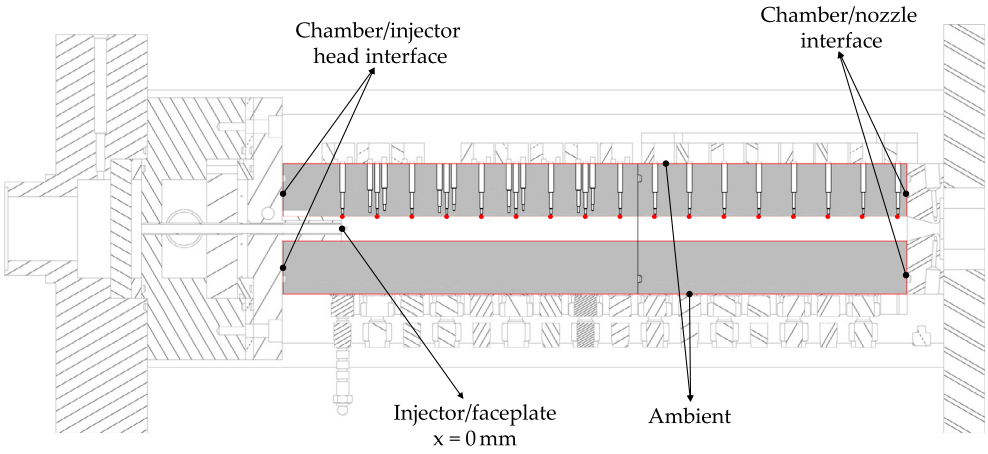

Fig. 2. Computational domain chosen for the inverse heat conduction method.

representation of the geometry constitutes the code very efficient from a computational standpoint and allows the iterative solution of the heat transfer problem in reasonable time.

The simplified computational domain is shown in Fig. 2 upon the example of a multi-element chamber. The grey area represents the computational domain and the red frame shows the boundaries. The thermocouple holes are also ignored in the computational model and the structure is modeled as a full-material block. The red points indicate the positions of the parameter points in the optimization problem, which are located at the axial positions of the thermocouples, projected onto the hot gas wall. Note that the computational domain in the presented method is three-dimensional and Fig. 2 shows only a 2D slice of the domain.

Apart from the boundary condition in contact with the hot gas, which is the sought variable, all the others must be defined a priori and are modeled with von Neumann and Robin boundary conditions. Specifically, an adiabatic boundary condition is used for the interface between the copper chamber and the injector head, whereas a natural convection boundary condition is applied to the outer wall with a convective heat transfer coefficient $h = 10\mathrm{W}/(\mathrm{m}^2 \cdot \mathrm{K})$and an ambient temperature corresponding to the one measured at each test.

For the boundary condition at the interface between combustion chamber and nozzle, an extensive sensitivity analysis has been performed. Specifically, an adiabatic boundary condition was compared to a time and spatially dependent heat flux, obtained by simulations performed with the in-house tool Thermtest [17]. The analysis resulted to the conclusion that the choice of this boundary condition has very small influence on the final heat flux profile. Specifically, between the solutions with the adiabatic and the Thermtest boundary condition, a maximal deviation of $\sim 5\%$ was observed in the heat flux value at the location of the last downstream thermocouple. All other positions upstream appeared to be unaffected by the choice of boundary condition, proving the low sensitivity of the final result on the treatment of this interface. For that reason and to ensure that the rebuilding of the thermal field is purely done on the basis of the measurements without relying on other inputs such as thermal simulations of the nozzle, an adiabatic boundary condition is imposed.

Upon solving the direct problem, the temperature field at the end of the first time step is known. The calculated value of the temperature at all the thermocouple positions can hence be extracted and compared with the measured ones. This residual temperature difference is given as an input to the optimization algorithm.

Fig. 3 shows a slice of the computational grid in the example of the rectangular single-element chamber. Only the upper-right quarter of the cross-section is shown due to the symmetry but the computational domain consists of the full chamber. A uniform spacing is used both in horizontal and vertical directions. Note than only every second node is shown in the figure for visualization purposes. In axial direction, a uniform spacing is used for the nodes, with a distance of 0.5 mm between neighboring nodes. The resolution was chosen after an extensive grid convergence study. In Fig. 3, the positions of the thermocouples at 1 mm, 2 mm and 3 mm from the hot gas wall are shown (blue points), as well as the projected parameter location (red point) as will be described in Section 2.2.

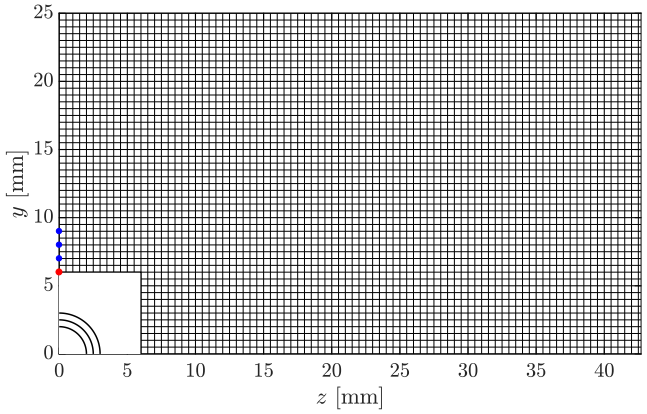

Fig. 3. Computational grid for the rectangular single-element chamber (every second node is shown).

2.2. Optimization method

The purpose of the optimization is to minimize the difference between the calculated ($\mathbf{T}_c$) and measured ($\mathbf{T}_m$) temperatures at each time step. This residual J which is subject to minimization is defined as in Eq. (2):

$$J(\mathbf{P}) = [\mathbf{T}_m - \mathbf{T}_c(\mathbf{P})]^T [\mathbf{T}_m - \mathbf{T}_c(\mathbf{P})] \tag{2}$$

The vector $\mathbf{P}$ describes the heat flux values at the parameter points which are subject to optimization. The heat flux is a continuous variable being applied to all the points, however optimizing the heat flux value at every single point in contact with the hot gas would be computationally expensive and render the problem more ill-posed [18]. Having a larger number of optimization points increases the degrees of freedom of the problem without

increasing the information input (no additional thermocouple measurements). For that reason, for the method presented here, a parameter is placed only at locations which possess at least one temperature sensor, so the number of parameters N is always smaller or equal to the thermocouple number M. At each time step, the values of the N parameter points are changed to reduce the residual J.

For the determination of the amount by which each parameter value should be modified at every iteration, two separate methods have been applied and compared. Both of them are based on an iterative update by means of the Jacobi matrix $\mathbf{S}$, which serves as a sensitivity matrix describing the change of the temperature at a thermocouple position due to a small change at a specific heat flux parameter value. Its structure is presented in Eq. (3). It was shown in a sensitivity study that the linearity of the Fourier heat conduction equation allows for a calculation of the Jacobi matrix outside of the optimization loop. For that reason the computation of the matrix for both methods occurs as a pre-processing step before the calculation and it is saved for future calculations as well. As long as the number and locations of the thermocouples and parameters does not change, the matrix remains unaltered.

$$\mathbf{S} = \begin{bmatrix} \frac{\partial T_1}{\partial P_1} & \cdots & \frac{\partial T_M}{\partial P_1} \\ \vdots & \ddots & \vdots \\ \frac{\partial T_1}{\partial P_N} & \cdots & \frac{\partial T_M}{\partial P_N} \end{bmatrix} \tag{3}$$

The first method relies on a conjugate gradient method as described in Özisik [19]. After each iteration k, the values $\mathbf{P}^k$ are updated according to Eq. (4).

$$\mathbf{P}^{k+1} = \mathbf{P}^k - \beta^k \cdot \mathbf{d}^k \tag{4}$$

where β^k represents the search step size and $\mathbf{d}^k$ the direction of descent of the conjugate gradient method. Using the Fletcher-Reeves [20] expression for the conjugation coefficient and the gradient of the residual function from Eq. (5), the closure of the optimization algorithm is given by Eqs. (6)–(8) as described in Özisik [19].

$$\nabla J(\mathbf{P}^k) = -2[\mathbf{S}]^T \left[\mathbf{T}_m - \mathbf{T}_c(\mathbf{P}^k)\right] \tag{5}$$

$$\mathbf{d}^k = \nabla J(\mathbf{P}^k) + \gamma^k \mathbf{d}^{k-1} \tag{6}$$

$$\gamma^k = \frac{\sum_{j=1}^{N} \left[\nabla J(\mathbf{P}^k)\right]_j^2}{\sum_{j=1}^{N} \left[\nabla J(\mathbf{P}^{k-1})\right]_j^2} \tag{7}$$

$$\beta^k = -\frac{\left[\mathbf{S}\mathbf{d}^{\mathbf{k}}\right]^T \left[\mathbf{T}_m - \mathbf{T}_c(\mathbf{P}^k)\right]}{\left[\mathbf{S}\mathbf{d}^{\mathbf{k}}\right]^T \left[\mathbf{S}\mathbf{d}^{\mathbf{k}}\right]} \tag{8}$$

The second method is based on a linearization of the problem and follows the Newton-Raphson formulation for the solution of non-linear systems [21]. The heat flux at each iteration step is obtained by solving the algebraic equation

$$\mathbf{S} \cdot \mathbf{P}^{k+1} = \left[\mathbf{T}_m - \mathbf{T}_c(\mathbf{P}^k)\right] + \mathbf{S} \cdot \mathbf{P}^k \tag{9}$$

In both cases, the process is repeated until convergence is achieved, i.e. until the residual drops beneath a predefined value ϵ. When this is the case, the calculation of the next time step takes place while the temperature is initialized with the converged temperature field of the previous time step. The stopping criterion ϵ was chosen to be proportional to the precision of the thermocouple measurements ΔT, to the time step Δt and the number of the thermocouples M using an empirical constant C. Due to the inherent uncertainty of the thermocouple measurements, the error ΔT was set to the accuracy of the used temperature measurement system.

$$\epsilon = C \cdot M(\Delta T)^2 \Delta t \tag{10}$$

It has been shown that both methods delivered identical results for the converged heat flux. However, the number of iterations required until convergence is lower by a factor 3 in the case of the Newton-Raphson method. For that reason this method is utilized for all results presented in Section 6.

2.3. Applying the heat flux on the boundary

As mentioned in the description of the optimization algorithm, the heat flux is updated only at specific locations and specifically only at the thermocouples' positions projected on the hot gas wall. Special care has to be taken to transform the heat flux from the few locations in the chamber to a continuous variable over the whole boundary domain. A cubic interpolation is used to transform the discrete values to a continuous profile in axial direction. However, the treatment along the perimeter is done differently for the single-element and multi-element configurations and will hence be described in Section 6.

3. Experimental setup

The inverse heat conduction method presented in this work was initially developed with the purpose of evaluating the experimental heat flux stemming from the hot runs of capacitively cooled rocket combustors operated at the Space Propulsion Division (RFA) of the Technical University of Munich (TUM). Within the framework of the German National Science Foundation (DFG) the DFG-TRR40 project entitled Fundamental Technologies for the Development of Future Space-Transport-System Components under High Thermal and Mechanical Loads has been funded, aiming at increasing the experience around the propellant combination methane/oxygen for future space applications [4].

In particular, the Space Propulsion Division of TUM has been working with these propellants for the last seven years employing different model combustors to provide detailed data about injector/injector and injector/wall interaction both for furthering identification and quantification of key phenomena and processes and for validation of engineering design tools [22,23]. For an optimum cooling system and specifically the cooling channel design it is essential to know in sufficient detail the axial and azimuthal heat load distributions for a particular injector geometry and their sensitivity towards variations of the operating condition.

In order to achieve these goals with a reasonable effort the following approach has been taken. In a first phase several single injector combustors (circular and square cross section and the later with an optional optical access to allow visualization of the near injector region) have been applied to investigate initial phenomena such as injector/wall interaction, combustion efficiency, film cooling and flow field from the injector with recess. In a second phase multi-injector combustors with rectangular and circular cross section have been operated to look additionally into injector/injector interaction and the effect of a smaller ratio of combustor surface to combustor volume.

For the evaluation of the heat flux profiles from the experiment, the RoqFITT code has been developed and applied to the different thrust chambers of the TUM. The object of the current investigation are the circular single-element, square single-element and rectangular multi-element rocket combustors, which are operated without an active cooling system and are hence subject to transient

temperature profiles within their structure. An overview of the hardware can be seen in Figs. 4–6 respectively.

All the model combustors are equipped with identical injectors, similar injector/wall distances and injector/injector distances and have the same contraction ratio ϵ_c. Due to the gaseous nature of the propellants such a design allows for similar injection velocities independently of combustion chamber pressure p_c, for similar chamber Mach numbers ($Ma \approx 0.25$) and thus convective transport characteristics and similar characteristic mixing lengths. For more information about the different combustors, see [24–27].

In all three of the examined combustors, type T thermocouples with 0.5 mm diameter are installed to measure the temperature within the oxygen-free copper material (Cu-HCP) of the structure. These measurements serve as the input for the inverse method, which aims at minimizing the error between the calculated and measured temperature signal for all time steps. The thermocouples are positioned at 1 mm, 2 mm and 3 mm distances from the hot gas walland their axial resolution is 17 mm. In the case of the circular and square single-element chambers, only one thermocouple is installed per plane, located directly above the injector element. The multi-element chamber can potentially accommodate up to seven thermocouples per axial plane, in order to measure the heat flux footprint created by the presence of five injector elements. As shown in the right sub-figure of Fig. 6, thermocouples are installed above each one of the five injectors and two additional ones are present left and right of the central injector element, right between two neighboring elements.

4. Error analysis

For a proper evaluation of the experimental data and a potential comparison with CFD simulations, knowledge of the different error sources as well as the magnitude of the individual errors is necessary. The error sources are usually due to statistical and systematical error of the measured data as well as due to the uncertainties used in the models.

In the case of the RoqFITT code the measurements are restricted to the thermocouple readings. As far as the model is concerned, RoqFITT uses the heat conduction equation with proper boundary conditions. The potential error sources are hence the material properties and the treatment of the boundary conditions at the interface with the nozzle as well as with the ambient environment.

Summarized, the uncertainties which have to be included in the error propagation are the following:

- Thermocouple accuracy
- Thermocouple precision
- Thermocouple positioning
- Thermocouple response delay
- Material properties
- Boundary conditions

The terms “accuracy” and “precision” are used in this context according to the definition by Taylor [28]: “accuracy” of a measurement is the deviation from the quantities “true value”, whereas “precision” refers to the reproducibility and repeatability of the measurement, i.e. the degree to which repeated measurements under unchanged conditions show the same results.

4.1. Thermocouple accuracy

For the accuracy of the thermocouples, the manufacturer’s instrument accuracy ΔT_{acc} can be used. Since the heat flux in the solution of the transient inverse problem is calculated based not on the absolute values of the temperature but in the form of a temperature increase within a time window, the total temperature error due to the instrument accuracy is doubled and hence has the magnitude $2 \cdot \Delta \mathbf{T}_{acc}$. Using the concept of linearization, the heat

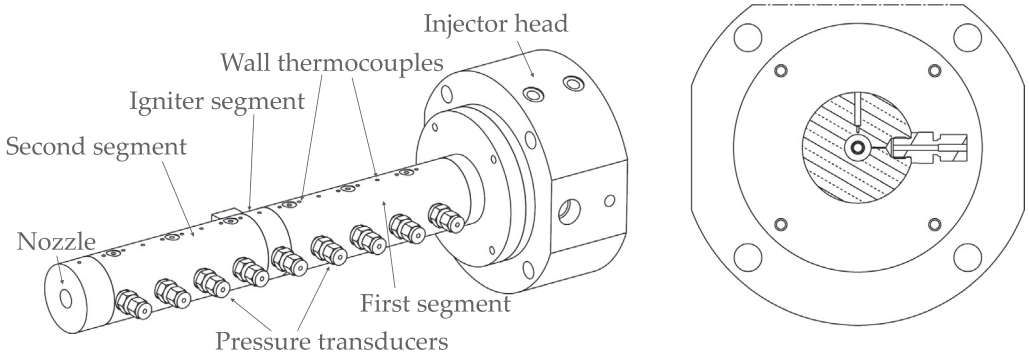

Fig. 4. Circular single-element combustion chamber hardware.

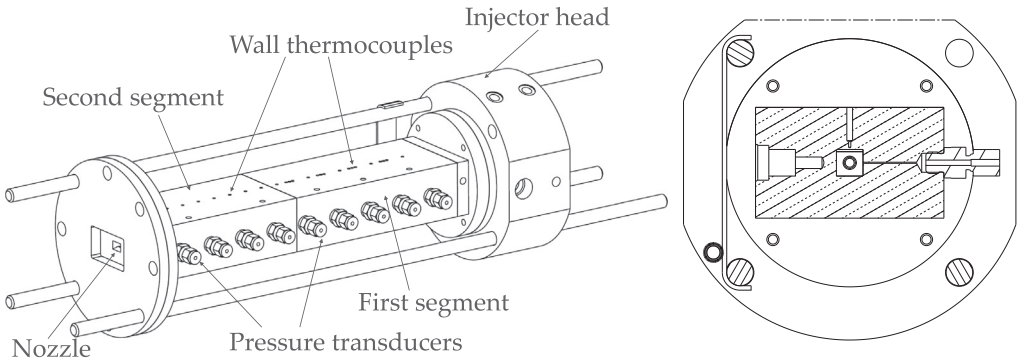

Fig. 5. Square single-element combustion chamber hardware.

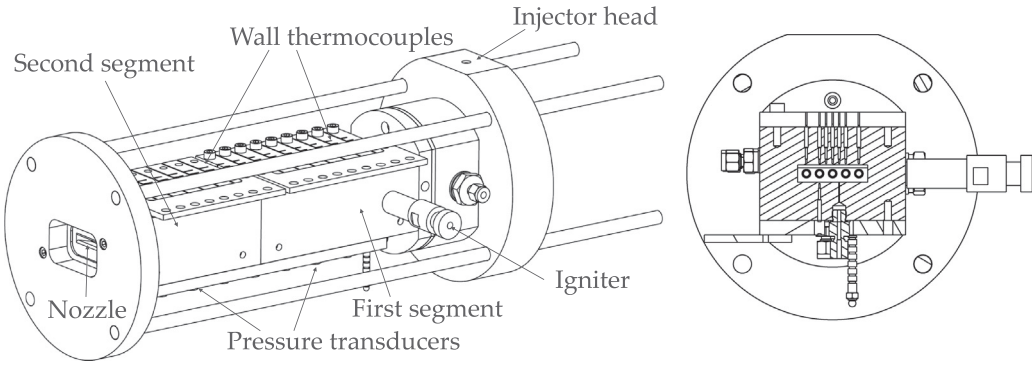

Fig. 6. Multi-element combustion chamber hardware.

flux error $\Delta\mathbf{P}_{acc}$ can be obtained by means of the Jacobi matrix, by solving the algebraic system in Eq. (11).

$$\Delta\mathbf{P}_{acc,i} = 2 \cdot \mathbf{S}^{-1} \cdot \Delta\mathbf{T}_{acc,i} \tag{11}$$

where the index i denotes the i-th time step.

4.2. Thermocouple precision

In case of the transient temperature measurements, the precision error is defined as the random fluctuation of the thermocouples readings. The raw thermocouple data is prone to high frequency noise and for that reason the transient profiles are smoothened before the start of the inverse method. The difference between the smoothed signal and the raw data is defined as the precision error and the corresponding heat flux error is defined as in Eq. (12)

$$\Delta\mathbf{P}_{prec,i} = \mathbf{S}^{-1} \cdot \Delta\mathbf{T}_{prec,i} \tag{12}$$

4.3. Thermocouple positioning

One of the largest sources of uncertainty when using thermocouples is the fact that their exact location is not always known. In order to take this into account, a post-processing step is introduced in RoqFITT, during which a systematic spatial deviation Δy is defined for all thermocouples. The initial position of the thermocouples y_0 is hence replaced by $y_0 + \Delta y$. Using the converged solution for the heat flux and the temperature field in the domain, the temperature at the new thermocouple positions can be found and it is used for the estimation of the temperature error:

$$\Delta\mathbf{T}_{loc,i} = \mathbf{T}_{c,i}(y_0) - \mathbf{T}_{c,i}(y_0 + \Delta y) \tag{13}$$

A maximal deviation equal to 0.5 mm is used for all hardware. The estimation of the resulting heat flux error is carried out with the Jacobi matrix similar to Eq. (12).

4.4. Thermocouple response delay

Apart from the position of the thermocouples, their thermal contact with the chamber material and their thermal inertia are not always ideal. Specifically, the combined effect of the contact thermal resistance (R_t) and the heat capacity (C_t) of the sensor give rise to a response delay time of each thermocouple $\tau = R_t \cdot C_t$. Any change in R_t and C_t will cause a body to respond differently to any changes in its thermal environment. Such a delay has to be taken into account when evaluating the heat flux for a capacitive hardware, since the measured temperature continues to increase after the combustion starts, resulting in unsteady temperature and heat flux at the wall. Because of the delayed response of the thermocouples, there is some discrepancy between the real time temperature and the experimental output.

In order to quantify the error resulting from the response delay time, the method presented by Wang et al. [29] is implemented, according to which, the real temperature at the thermocouple position T_{real} is related to the measured thermocouple output T_{meas} according to:

$$\frac{dT_{meas}}{dt} = \frac{T_{real} - T_{meas}}{\tau} \tag{14}$$

The effect of the response delay time on the measured thermocouple temperature is illustrated in Fig. 7. The thermocouple reading corresponds to $\tau = 0$ ms and represents the actual output without correction. The corrected temperature profiles for different values of the response delay are also shown in Fig. 7 and have larger values than the measured temperature for the entire duration of the experiment.

Typical response time values for 0.5 mm type T thermocouples are between 100 and 200 ms [15,29]. In the present study all thermocouple readings are corrected using Eq. (14) and a value of $\tau_0 = 100$ ms is assumed.

To estimate the heat flux uncertainty resulting from the thermocouple contact resistance and thermal inertia, Eq. (15) is used. The modified thermocouple measurement using the standard delay time τ_0 is compared to an increased standard delay time $\tau_0 + \Delta\tau$ and the heat flux error is obtained with the use of the sensitivity matrix. In the present framework a value of $\Delta\tau = 100$ ms is chosen.

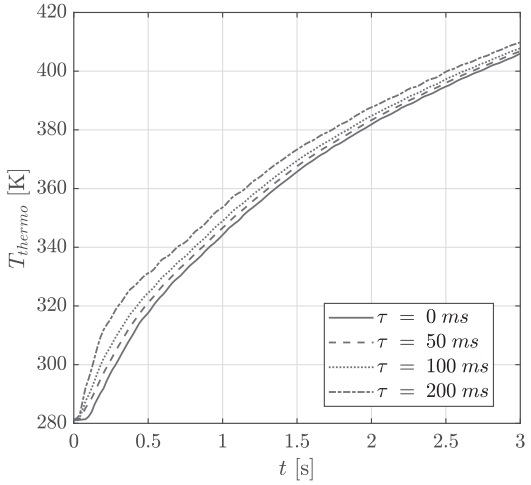

Fig. 7. Comparison of "real" and measured temperature at thermocouple position for different response delay times.

$$\Delta \mathbf{P}_{res,i} = \mathbf{S}^{-1} \cdot \Delta \mathbf{T}_{res,i} = \mathbf{S}^{-1} \cdot \left(\mathbf{T}_{m,i}(\tau_0) - \mathbf{T}_{m,i}(\tau_0 + \Delta\tau) \right) \tag{15}$$

4.5. Material properties

The material properties used in the solution of the direct problem are taken from the data sheet of the combustion chamber material. However there is some uncertainty connected to the choice of the thermal conductivity, density and heat capacity and for the quantification of its effect on the converged heat flux values is important.

The procedure for the calculation of the material-induced error goes as follows: Upon convergence of the inverse method, the converged heat flux values are used as input for the solution of a direct problem. In this direct problem however, the thermal diffusivity is replaced by a value which is modified compared to the nominal value α_0. The magnitude of the deviation $\Delta\alpha$ was estimated at 10%. The resulting heat flux error for each time step is simply given by Eq. (16).

$$\Delta \mathbf{P}_{mat,i} = \mathbf{S}^{-1} \cdot \Delta \mathbf{T}_{mat,i} = \mathbf{S}^{-1} \cdot \left(\mathbf{T}_{c,i}(\alpha_0) - \mathbf{T}_{c,i}(\alpha_0 + \Delta\alpha) \right) \tag{16}$$

4.6. Boundary conditions

In the computational domain of the rocket combustors shown in Fig. 2, the boundary conditions at the surfaces in contact with the nozzle and the outer surface have to be modeled. The natural convection was found to have a negligible effect on the final result of the hot gas heat flux and is hence not included in the error propagation analysis.

For the nozzle interface the adiabatic condition has been compared to a spatially and temporarily varying nozzle heat flux which is obtained by means of the in-house tool Thermtest [17]. Thermtest allows the simulation of steady as well as transient thermal behavior of cooled or uncooled structures over a wide scope of chamber materials and cooling fluids. While the heat conduction inside the chamber material is solved by a 3D finite difference method, the convective heat transfer from the hot gas side to the inner wall as well as for the coolant is modeled using empirical Nusselt correlations. The approximated thermal field at the interface between nozzle and combustion chamber stemming from the Thermtest simulation can be used to deduce the value of the conductive heat flux. This is applied directly as a von Neumann boundary condition in RoqFITT.

To quantify the uncertainty of this value, a comparison of the results with the nominal nozzle heat flux $\dot{q}_{noz,0}$ (=0, due to adiabatic conditions) was performed with the assumed deviation $\Delta\dot{q}_{noz}$ stemming from Thermtest. The resulting error in the heat flux parameters $\Delta \mathbf{P}_{noz,i}$ can be determined as in Eq. (17):

$$\Delta \mathbf{P}_{noz,i} = \mathbf{S}^{-1} \cdot \Delta \mathbf{T}_{noz,i} = \mathbf{S}^{-1} \cdot \left(\mathbf{T}_{c,i}(\dot{q}_{noz,0}) - \mathbf{T}_{c,i}(\dot{q}_{noz,0} + \Delta\dot{q}_{noz}) \right) \tag{17}$$

An extensive analysis showed that only the heat flux at the parameter point closest to the interface is influenced but the effect is kept below 10% even for large nozzle heat flux values.

Summing up all the error sources according to Eq. (18) results in a total uncertainty between 10% and 15% of the converged heat flux value at each parameter location.

$$\Delta \mathbf{P}_{tot,i} = \sqrt{\Delta \mathbf{P}^2_{acc,i} + \Delta \mathbf{P}^2_{prec,i} + \Delta \mathbf{P}^2_{loc,i} + \Delta \mathbf{P}^2_{res,i} + \Delta \mathbf{P}^2_{mat,i} + \Delta \mathbf{P}^2_{noz,i}} \tag{18}$$

The main contribution (around 80%) results from the thermocouple positioning and response delay time, whereas the boundary condition and precision errors are negligible.

4.7. Hot gas wall temperature error

Apart from the heat flux profile at the inner wall of the combustion chamber, a further result of the inverse heat conduction method is the wall temperature at the positions in contact with the hot gas. This is usually utilized as the thermal boundary condition in CFD simulations and is an important figure for the estimation of the engine's lifetime. Hence, knowing the uncertainty of the calculated values is also quite important.

This can be performed by means of the Jacobi matrix, estimated directly at the hot gas positions. With this information, the temperature errors at the hot gas can be evaluated by:

$$\Delta \mathbf{T}_{hot\,gas,i} = \mathbf{S}_{hot\,gas} \cdot \Delta \mathbf{P}_{tot,i} \tag{19}$$

Of course this implies the calculation of a second Jacobi matrix $S_{hot\,gas}$, which can be computationally expensive.

5. Validation

Before the application of the code to the evaluation of experimental data, a validation was carried out. Specifically, a validation of the direct solver and the inverse algorithm as well as a validation of the inverse method as a whole was performed.

5.1. Algorithm validation

For the validation of the direct solver, a comparison of the resulting temperature distribution given a specific heat flux as boundary input was done between RoqFITT and the commercial tool ANSYS [30]. The temperature results matched within an accuracy of 0.5 % leading to the conclusion that the direct solver is reliable.

For the validation of the inverse algorithm several tests were carried out. The purpose of the inverse algorithm is to determine the (unknown) applied heat flux based on temperature readings. Hence, to validate it, one has to provide measurements obtained with a precisely defined boundary condition. If the results from the inverse algorithm agree with the pre-defined conditions, then the algorithm can be considered as validated.

In the following, a time and spatially variable heat flux profile is applied to the hot gas wall of the square single element chamber. The profile is illustrated in Fig. 8 and is chosen with typical characteristics as the expected heat loads within the experimental combustor. Specifically, a transient increase of the heat flux level within the first second of operation is defined. Within this period, a small oscillation is imposed, resembling the effect of the igniter, which is located in the middle of the chamber. The effects of

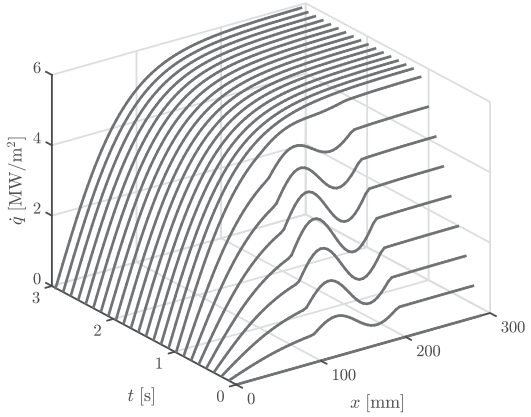

Fig. 8. Heat flux profile applied at the chamber wall for the validation.

ignition are usually measured within the first 0.5–1 s of the combustion tests. After the initial start-up, a steady state profile is obtained for the heat flux, which shows larger values for positions downstream of the injector and a subsequent constant plateau after approximately 200 mm from the faceplate. This resembles typical axial heat flux distributions where the heat flux increases for the first part of the combustion chamber since the mixing and energy release is not complete before reaching a nearly constant value upon completion of the combustion process. No variation of the heat flux is defined along the circumference of the square wall, i.e. a constant heat flux is applied for each axial position.

Using the profile from Fig. 8 a direct problem is run and the temperature values at the sensor locations are obtained. Using a random error of 0.5 K for the temperature data (to resemble the experimental noise), the "experimental" data are prepared. Those serve as input for the inverse heat conduction method. For the optimization, 18 parameters are used, located at the same axial locations as the thermocouples. The resulting heat flux profiles for some representative time steps are compared to the imposed ("direct") boundary condition (BC) in Fig. 9. Both the transient as well as the spatial variation is reproduced by the inverse method, with the maximal errors at the optimization positions remaining below 5%. During the steady state heat flux level, the errors were kept at below 1% and result mainly from the artificial thermocouple error imposed.

5.2. Method validation

The single-element chambers presented in Sections 6.1 and 6.2 can only be operated in capacitive mode and hence no available calorimetric measurements are available for comparison. Such comparison is however possible for the multi-element chamber and can be used for the validation of the inverse heat flux measurement. The multi-element chamber can be operated either in capacitive or in water-cooled mode. This is enabled by the modular form of the chamber segments which can be interchanged. In the water-cooled configuration, the segments are equipped with cooling channels which can be flown either counterflow or in co-flow with the hot gas. This makes a measurement of the heat flux based on the enthalpy difference of in- and outflowing water possible.

A test at O/F = 3.4 and pressure of 20 bar carried out once with the cooled hardware and once with the capacitive one is shown in Fig. 10. The test is taken from Perakis et al. [16]. Seven water-cooled separate segments are present, which provide the average heat flux for each one of them. In order to perform the comparison,

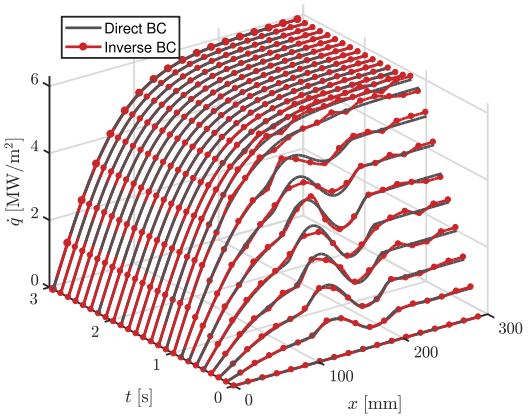

Fig. 9. Comparison of imposed direct boundary condition and resulting inverse boundary condition from RoqFITT.

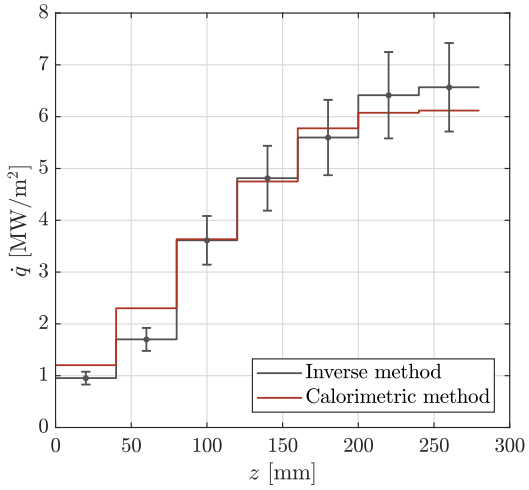

Fig. 10. Comparison between experimental heat flux obtained with the inverse and calorimetric method.

the results from the inverse method are also averaged along the same positions. It can be observed that the two curves demonstrate the same trend and have a difference of less than 3% in the segments located close to the middle of the chamber.

Planes closer to the injector plane and the nozzle show a higher deviation, which however remains within 7% with the exception of the second segment. The calorimetric method also contains some uncertainty which has not been quantified in the original experiment. Moreover, although efforts are made that the two hardware configurations (capacitive and water-cooled) are identical, it is still two different pieces of hardware and some discrepancies in the results could be attributed to this fact (slightly different material properties, installation of thermocouples etc.). The general trend however of the two methods is in good agreement, serving as a first validation of the inverse method.

6. Results

Selected results using the RoqFITT code for the evaluation of the heat flux profiles in the combustion tests of the hardware presented in Section 3 are outlined in this chapter. The main purpose is to demonstrate the capabilities of the code as far as the calculation of the heat loads is concerned. However, at the same time an investigation of the physical phenomena is given in order to explore whether the obtained heat flux values agree with the expected physical and chemical phenomena taking place within the chamber.

6.1. Circular single-element combustor

The single-element combustor shown in Fig. 4 can be operated either with CH_4/O_2 or H_2/O_2 in gaseous phase and at operating pressures up to 30 bar. The test operation is restricted to 3 s to avoid thermal and mechanical damage of the structure. For the estimation of the heat flux, thermocouples are installed at 17 positions, equally distributed along the axis of the chamber, with an axial separation of 17 mm from each other. The thermocouples used for the inverse method are located at 1 mm distance from the hot gas wall. Due to the axisymmetric nature of the problem, a uniform heat flux is applied along the perimeter for each axial position. The interpolation between the discrete parameter values occurs with a cubic scheme.

The only information available used by the inverse method for the reconstruction of the thermal field are the transient

thermocouple readings at distinct positions in the material. The transient readings at selected positions are presented in Fig. 11, where the solid lines represent the calculated values and the dashed lines the experimental ones. In the right sub-figure, the corresponding difference between the two is also shown. One observes that the inverse method is capable of reconstructing the temperature values at the thermocouple locations within an accuracy of approximately 2 K. Specifically, the largest discrepancy occurs during the initial sharp temperature rise due to the start of the experiment, while after 1 s of operation the difference between the two values is close to 1 K for most sensors. The data shown in Fig. 11 are from a CH_4/O_2 test at 20 bar and O/F = 3.0.

Due to the capacitive nature of the test hardware, the temperature profile is transient and does not reach a steady state within the 3 s of operation. A typical time-evolution of the pressure signal and a thermocouple measurement in the chamber is shown in the left sub-figure of Fig. 12. The valves are opened at 0 s and the combustion in the chamber takes place for approximately 3 s. During this duration, the pressure signal reaches a steady state shortly after the begin of the test and then oscillates around the nominal value. The temperature signal on the other hand steadily increases over time until the shut-off. The inverse method deals only with the time window of the test, i.e. only for the first 3 s of operation and hence the thermocouple readings within this time frame are taken as inputs.

Both the temperature and the heat flux however are transient values and in order to carry out an evaluation of the axial profiles of these values, an evaluation window must be chosen. In the present work this is done at 2/3 of the operational duration (i.e. at $t = 2$ s) and the window width is 0.5 s, when the pressure and heat flux profiles reach a steady state. The values within this window are averaged and can give insights about the axial distribution of heat loads. Although this method is described for the round single-element chamber in this section, it is the procedure followed for all three hardware. Some exemplary heat flux values at different axial positions are plotted over time in the right sub-figure of Fig. 12. It is evident that the initial start-up transient leads to an increasing heat flux for the first second of operation but after that an almost steady value is predicted in each position. Hence the choice of the evaluation window in the interval 2–2.5 s is justified, since within it the heat flux values are almost constant.

Using the inverse heat conduction method, important insights into the different heat loads stemming from the various propellant properties and pressure levels can be extracted. In Fig. 13, a comparison between the predicted heat flux results using H_2/O_2 and CH_4/O_2 at 10 and 20 bar nominal chamber pressure is shown. An

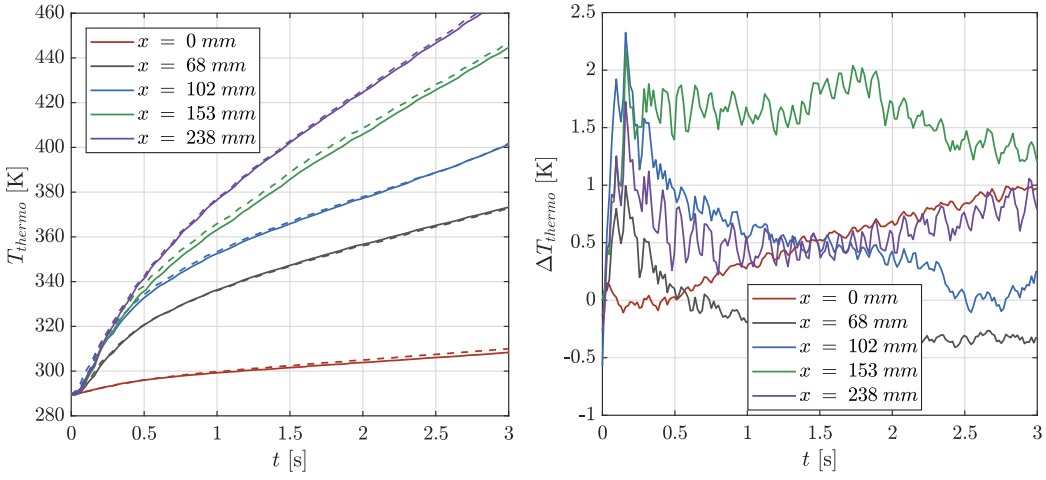

Fig. 11. Transient profiles of the calculated and measured temperature at selected thermocouple positions (left) and the corresponding difference between calculated and measured values (right) for the round chamber.

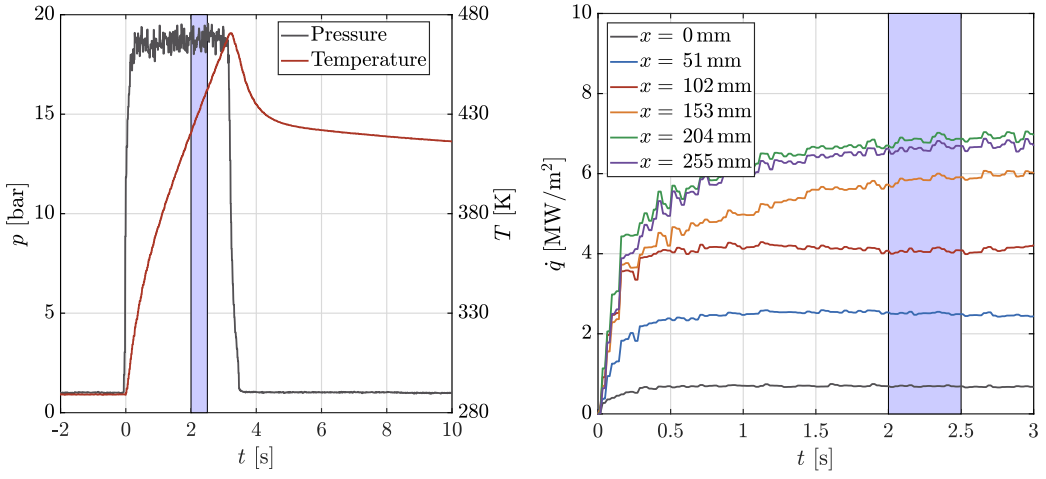

Fig. 12. Temperature, pressure and heat flux profiles along time. The evaluation window is indicated in blue color. (For interpretation of the references to colour in this figure legend, the reader is referred to the web version of this article.)

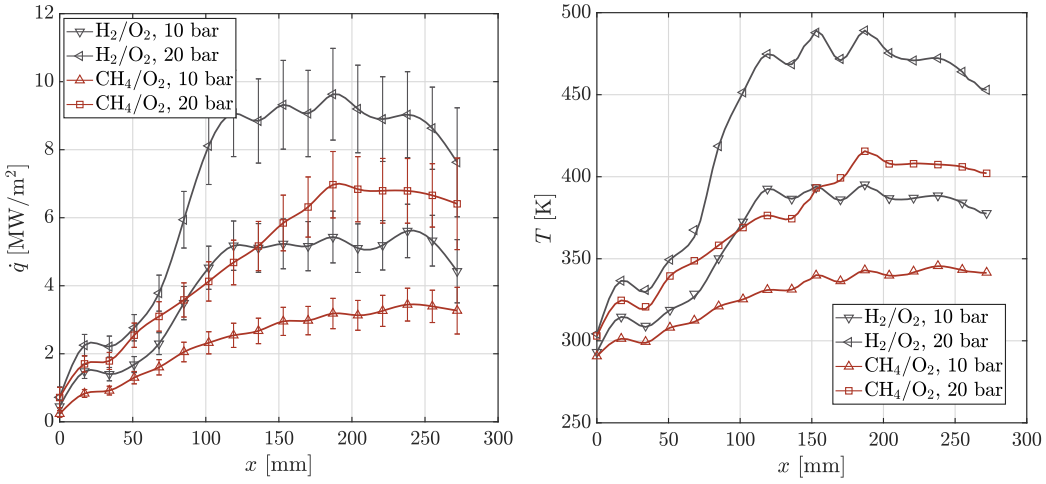

Fig. 13. Axial heat flux and temperature profile for H_2/O_2 and CH_4/O_2 load points using the circular rocket combustor at the evaluation time. The temperature profiles correspond to a 1 mm distance from the hot gas wall.

extensive comparison of the experimental data with results from CFD simulations is given in Roth et al. [31]. The nominal oxidizer to fuel ratio (O/F) in the hydrogen case is equal to 6.0 and for methane equal to 3.0.

In the right sub-figure of Fig. 13, the measured temperature values at 1 mm from the hot gas wall are plotted with symbols, whereas the solid lines represent the calculated temperature distribution from the inverse method. The shown profiles correspond to the averaged values within the evaluation window shown in Fig. 12, i.e. between 2 s and 2.5 s. An excellent agreement between the two values is observed, as expected since the goal of the method is to minimize the difference between the two. A higher temperature is shown in the case of H_2/O_2 compared to CH_4/O_2 both at 10 and 20 bar. This correlates to a higher heat flux predicted by the inverse method as shown in the left sub-figure. The uncertainty of the heat flux profile when taking into account all the error sources from Section 4, reaches approximately 13% for the majority of the axial positions. For axial positions between 100 mm and 200 mm a wavy pattern is observed in the thermocouple measurements. This translates to a heat flux oscillation at the same locations. The wavy pattern is visible for all time steps and does not experience an oscillatory behavior in time. This effect is attributed to a systematic error in the installation of the thermocouples either in terms of positioning or thermal contact with the chamber.

The results of the inverse method allow for a quantitative examination of the effects of higher pressure on the heat loads. In order to investigate the plausibility of the obtained results, an effort is made to explain the profiles based on the expected physical phenomena in the chamber.

According to Bartz [32], the heat transfer coefficient in a rocket engine correlates almost linearly according to $h \sim p_c^{0.8}$ with the combustion pressure p_c. Extensive data from Pempie [33] show that the same relationship holds true also for the maximal heat flux level in most LOX/LH_2 engines. In the data presented here, a clear increase of the heat flux with increasing pressure is seen, for both propellant combinations. To examine the applicability of this relationship to the examined combustion chamber, a fit of the data from the inverse method is carried out, according to $\dot{q} = C \cdot p_c^n$. Estimating the parameter n for methane and hydrogen results in values of 0.93 and 0.81 respectively. Hence it is found that for both the gaseous methane and the gaseous hydrogen tests, the qualitative trend of the Bartz correlation holds true and an almost linear heat flux level increase is expected with larger combustion chamber pressure.

Despite the similarity regarding the absolute level increase, the heat flux profiles for the two propellant combinations present several differences. Regarding the heat loads, hydrogen presents higher heat flux values for both operating points, which can be easily understood as it is a more energetic propellant with a higher combustion temperature. As far as the axial profile is concerned, in the case of hydrogen, a sharp increase is observed starting around 50 mm from the faceplate, followed by an almost constant heat flux plateau which sets in at 110 mm. Subsequently, a drop in the heat flux is observed, which takes place close to the end of the chamber, namely at $x = 250$ mm. In the case of methane on the other hand, the heat flux increase takes place much slower, and a constant level is reached after approximately 200 mm.

The sharper increase in the case of H_2 can be attributed both to hydrodynamic as well as chemical effects. Due to the large density difference between oxidizer and fuel, a large velocity ratio is imposed, which facilitates the mixing in the gaseous phase. Specifically, the velocity ratio for the CH_4/O_2 configuration is close to 1, whereas for H_2/O_2 it approaches a value of 8. Hence due to the efficient mixing in the shear layer of the coaxial element, the energy release takes place much closer to the injector plane, leading to a steep heat flux rise. At the same time, the fast chemical reaction rates occurring in hydrogen combustion result in the energy release being finished earlier than in the case of methane. This explains why a steady plateau is obtained around the middle of the combustor, which indicates the end of combustion. Since no further reactions take place, the hot gas starts losing energy through the walls and this fact in combination with the thermal boundary layer build-up leads to a slight drop in heat flux. Due to the lower chemical rates of the methane combustion and the slower mixing, the heat release takes place gradually over the entire chamber length and the end of combustion occurs further downstream.

6.2. Square single-element combustor

The single-element combustor with square cross-section has been operated with CH_4/O_2 at different load points ranging from 5 to 30 bar and oxidizer to fuel ratios between 2.2 and 3.4 [26], different injector recess lengths [24] and with optical access using OH^* emission imaging [34]. For the estimation of the heat flux, thermocouples at 18 axial positions are available, equally distributed along the axis of the chamber, with an axial separation of 17 mm from each other. For some axial positions, thermocouples at 1 mm, 2 mm and 3 mm from the hot gas wall are available,

whereas at other positions only thermocouples at 1 mm from the wall are available. In total 24 thermocouples are used for the inverse method of this hardware.

The ability of RoQFITT to correctly reconstruct the thermal field is evident in Fig. 14. A test case of CH_4/O_2 at 20 bar and O/F = 3.0 is taken as an example. The calculated transient profiles at the locations of selected thermocouples (solid lines) are plotted as a function of time, along with the corresponding measurements (dashed line) and their respective deviation. Again, a very good agreement is observed.

Apart from the transient thermocouple readings, the ability of the code to predict the spatial distribution of temperature in the chamber is also interesting. In Fig. 15 the iso-lines of temperature are shown at the $x = 255$ mm plane at the evaluation time. It can be observed that despite the rectangular shape of the inner wall, the contours are nearly circular close to the hot gas wall. Further outwards, the effect of the capacitive corner takes place: a fast cool-down is observed towards the right and left edges due to the presence of a large copper mass. In the vertical direction on the other hand, less material is available which leads to higher temperatures and a slower cool-down rate.

With the established ability of the code to correctly reconstruct the temperature at specific points, an effort can be made to explain the obtained heat flux profiles based on the expected physical phenomena. In this section the heat flux and temperature profiles for three CH_4/O_2 experiments at 20 bar nominal operating pressure are presented. A comparison between the profiles of the three O/F ratios is illustrated in Fig. 16 and can be used for the characterization of the injector element. The heat flux profile is namely largely dependent on the mixing and energy release processes, which in the vicinity of the faceplate are dictated by the injector design.

The temperature profiles correspond to the inverse method results at a distance of 1 mm from the hot gas wall and the markers represent the measured thermocouple values. All plotted curves are the averaged results within the evaluation window shown in Fig. 12. It can be seen in Fig. 16, that the absolute level of the heat flux and temperature at the end of the combustion chamber is increasing with increasing O/F. This effect is expected, as the stoichiometric composition in the case of methane/oxygen combustion lies at a value of O/F $\approx$ 4.0. Around this value the highest heat release and the largest gas temperature are anticipated, leading to a larger heat loss to the wall.

In the vicinity of the faceplate however, the heat release is not only dictated by the chemistry but is largely influenced by the injector design. In the first 50 mm from the wall, an opposite trend is observed: the lowest O/F operating points seem to have a larger heat flux. This is an effect of the difference in velocity ratios among the tests. For the lowest O/F = 2.6, the methane flowing through the outer annulus has a larger velocity than oxygen. This larger velocity leads to a higher expansion angle of the jet and therefore to a shorter distance between the flame and the wall. This directly increases the heat input into the structure.

In a sense, the flame for smaller O/F values is closer to the faceplate compared to larger O/F, where the flame appears to have shifted downstream. This downstream shift is also evident when examining the heat flux increase close to the end of combustion. For O/F = 2.6, the heat flux appears to reach a constant value after approximately 255 mm, whereas for O/F = 3.4 the heat flux increases until the end of the chamber. This indicates a continuous heat release over the entire chamber length and hence an incomplete combustion. This feature is attributed to the lower momentum flux ratio ($\rho_{CH_4} v_{CH_4}^2 / \rho_{O_2} v_{O_2}^2$) at higher O/F. The higher momentum of oxygen pushes the mixing region further downstream and leads to this observed shift of the flame to positions closer to the nozzle. This effect was both measured with the optical imaging methods as well as reproduced in the CFD simulations

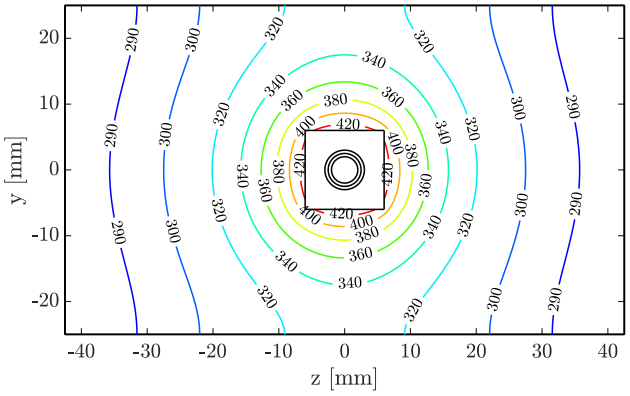

Fig. 15. Temperature field at the plane 255 mm downstream of the injector at evaluation time.

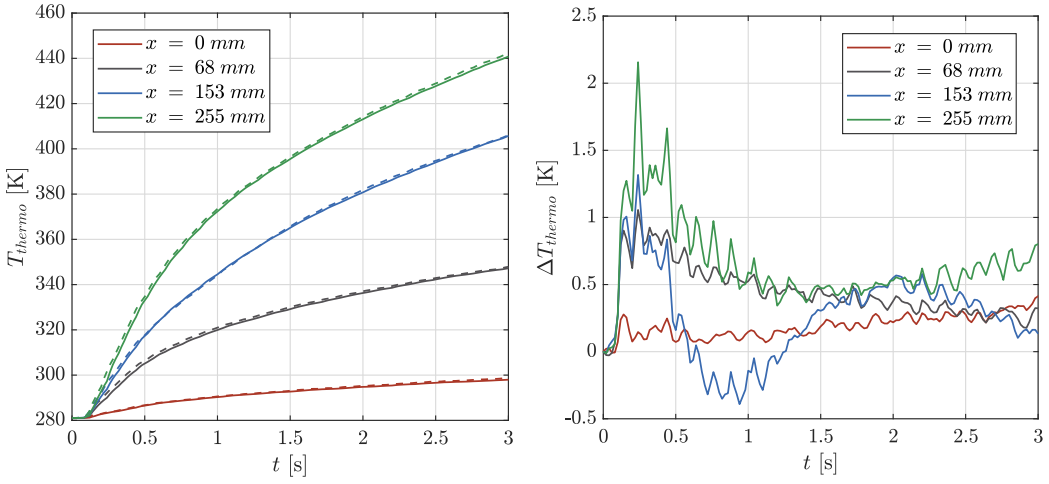

Fig. 14. Transient profiles of the calculated and measured temperature at selected thermocouple positions (left) and the corresponding difference between calculated and measured values (right) for the square chamber.

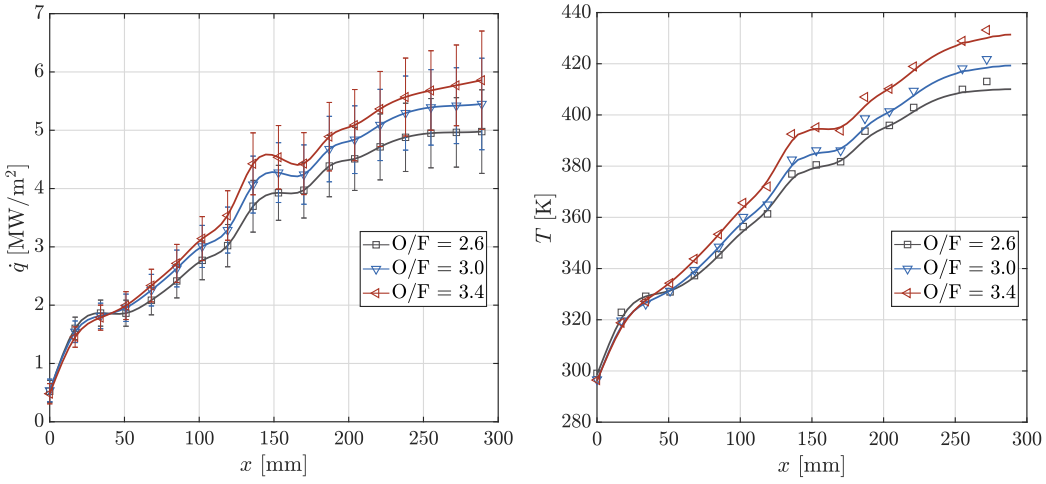

Fig. 16. Axial heat flux and temperature profile in the square single-element chamber for different operating points at the evaluation time.

presented in Winter et al. [34]. Hence using the inverse heat conduction method very significant information was able to be extracted from the available experimental data, essentially leading to a thorough understanding of the injector dynamics, mixing in gas phase and heat release.

In this evaluation, the optimization of the heat flux using RoqFITT occurs only at the specified parameter points, located at the positions of the thermocouples projected onto the hot gas wall. Along the perimeter of the rectangular cross section, a constant heat flux value is used. Physically, this assumption is not entirely motivating, since a lower heat flux is expected at the corners of the chamber due to the thermal boundary layer and the secondary flows, whereas the maximal heat flux should occur in the middle of each side. Due to the lack of further thermocouples in the present experimental configuration, no further information about the temperature outside of the middle plane is available, and hence no information about the heat flux distribution along the perimeter can be extracted.

An analysis has been carried out to examine the effect of the chosen heat flux profile along the perimeter. A large number of different profiles have been utilized, with all of them having a decreased corner heat flux value compared to the middle of the horizontal axis. It is namely expected that the heat flux approaches zero close to the corner. To demonstrate the effect of different profiles, the constant profile is compared to a variable profile, with the maximum placed in the middle of each side and the minimum of 0 at the corners. The shape of the profile is described by

$$\dot{q}(z) = \dot{q}_{max} \cdot \left(1 - \left(\frac{|2 \cdot z|}{w}\right)^n\right) \tag{20}$$

where w represents the width of the hot gas side and n a factor between 0 and 1 is.[1] Various values have been tested demonstrating similar results but for this study a value coming from the CFD simulation of the chamber in Winter et al. [34] is used with $n \approx 0.2$. For this comparison, the results of the test case with O/F = 3.0 are shown.

The results for the average heat flux along axial position are illustrated in Fig. 17. It can be seen that the two methods provide very similar distributions, with an offset which remains underneath 4% over the entire chamber length. Specifically, the variable profile predicts a slightly lower average heat flux compared to the constant one. This discrepancy can be better understood when examining the temperature and heat flux results of the inverse method along the spanwise direction (z axis) (see Fig. 18).

In the left sub-figure, it can be seen that both methods result in a maximal temperature in the middle of the horizontal side and minimal values at the sides. This is an effect created by the corners of the rectangular chamber, which act as a heat sink. Moreover, the temperature field with variable profile (dashed lines) shows a larger value at $z = 0$ mm. This is of course a result of the higher heat flux as shown in the right sub-figure. Although the temperature value directly at the wall is slightly higher with the variable profile, at 1 mm from the hot gas wall (i.e. at the location of the thermocouples) both methods deliver identical results by definition of the optimization problem. Due to the larger span-wise thermal gradient in the case of variable profile (steeper temperature drop towards the corners), the temperature decreases faster with increasing radial distance, leading to the same value with the constant profile at the measurement locations. Since the observed difference with both methods is so small however when evaluating the average heat flux values, both the variable and the constant profile are considered to be fully sufficient for this analysis.

6.3. Multi-element chamber

In contrast to the single-element combustors, in the multi-element one there is available information about the temperature values at more than one location in each axial position. As shown in Fig. 6, there is a maximal capacity of seven thermocouples per plane. Starting from left to right, the thermocouples are named 1C, 2C, 3L, 3C, 3R, 4C, 5C where "C" represents a position directly above an injector element, and "L", "R" the positions left and right of an element. Parameter points are placed at all the positions where thermocouple readings are available. It is important to note, that although seven measurements are possible at each plane, not all positions are equipped with thermocouples, and most planes possess only three measurements at 3L, 3C, 3R.

As mentioned in the description of the optimization algorithm, the heat flux is optimized only at specific locations and specifically only at the thermocouples' positions projected on the hot gas wall. Special care has to be taken to transform the heat flux from the few locations in the chamber to a continuous variable over the whole boundary domain. Along the z direction (horizontal side of the chamber), an interpolating procedure has to be implemented. A simple linear interpolation between two neighboring parameter values is in most cases prone to error. This is because locations named with the index "C" are directly above an injector element and are expected to have higher heat flux values (at least for loca-

[1] $z = 0$ mm corresponds to the middle of the horizontal side.

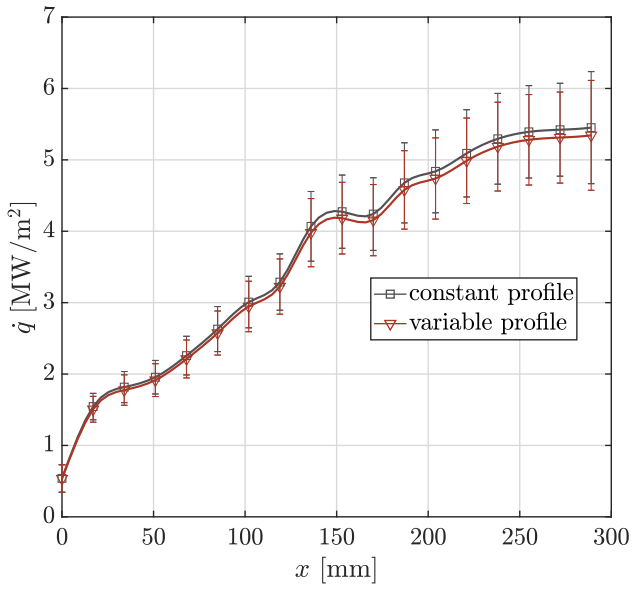

Fig. 17. Average heat flux profile for a constant and a variable distribution at the evaluation time.

tions close to the faceplate where the flame temperature's stratification is more dominant) compared to the locations between the two injectors (for example 3L). Hence a linear interpolation between 4C and 5C would be overestimating the flux between the injectors.

For that reason the heat flux at positions where the thermocouples are missing, are taken by averaging the remaining values at the same plane. This means that the missing values between the injectors 4 and 5 are taken by averaging the heat flux at 3R and 3L. In an analog fashion if the thermocouples at a position above an injector element are missing (e.g. 5C), then the average of the remaining central thermocouples are taken (e.g. 3C and 2C). This interpolation method assumes that the heat flux profiles above each one of the 5 injectors are similar for a specific plane. A cubic interpolation is used to convert the discrete parameter values to a continuous profile along the perimeter and the axial direction. Thermocouples are available at 16 equally spaced locations along the axial direction (separated by 17 mm from each other) and the total number of thermocouples used in the inverse method amounts to 66.

Only thermocouples at the upper wall are used and hence the heat flux profile at the bottom wall is defined identically to the upper wall, leading to a symmetric profile relative to the $y = 0$ plane. For the vertical walls of the hot gas side, a parabolic profile is defined. The corner value is known from the horizontal interpolation and the maximal value at the middle is defined as the average of the central values calculated for this plane (i.e. average of 1C, 2C, 3C, 4C, 5C). This can be used because the distance of the injector element from the vertical wall is the same as the one from the horizontal one, namely 3 mm.

Using those assumptions, the inverse method is used to evaluate a 20 bar, O/F = 3.4 CH_4/O_2 test case. The agreement of the calculated temperature values with the thermocouple readings is in accordance with the results presented in Figs. 11 and 14 for all sensor locations. Whereas the focus in Sections 6.1 and 6.2 was mainly on the axial profiles of the heat flux and temperature, in this section attention is specifically paid to the ability of RoqFITT to capture transient phenomena as well as information about the distributions along the perimeter.

Firstly, the pressure and heat loss profiles are compared in the left sub-figure of Fig. 19. The two variables are connected to each other since the combustion process has the effect of both raising the pressure within the chamber as well as increasing the energy release and hence the integral heat load to the wall. The values for the heat release calculated by the code refer only to the combustion chamber, excluding the nozzle since no heat flux values are available. The pressure measurement used here corresponds to the sensor located close to the faceplate, i.e. at $x = 0.5$ mm.

It is observed that the heat release starts increasing approximately at the same instant as the pressure at $t = 0$ s. After a sharp rise for the first 250 ms, the heat release increase seems to slow down at $t = 0.25$ s. The pressure profile also measures a small oscillation at the same time. The effect is attributed to the end of the igniter operation, which leads to a slight hold in the increase of the energy release. During the operation of the igniter, the presence of an additional transversal jet influences the injector flame, due to a local increase of mixing and therefore higher heat release, which is explained by the peak of the heat flux close to the faceplate. Immediately after the influence of the igniter is

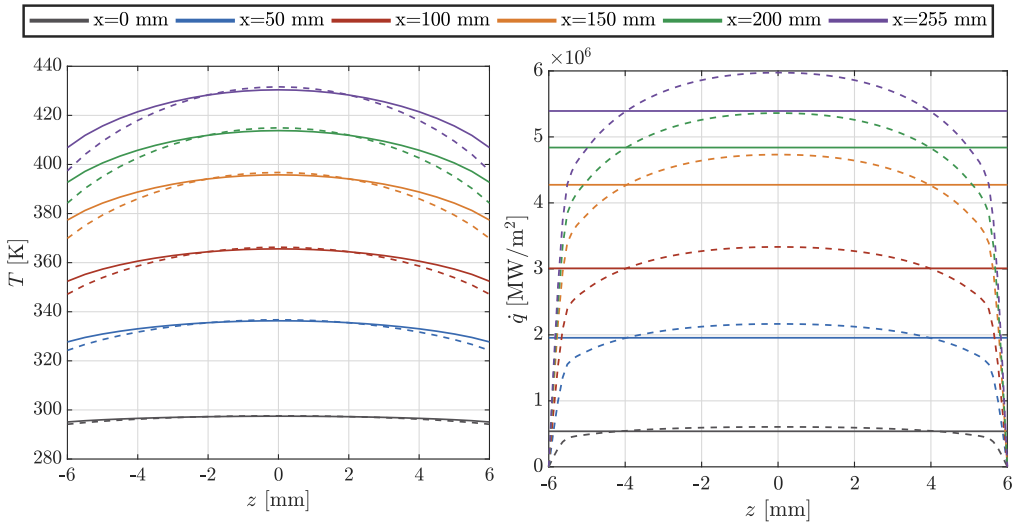

Fig. 18. Temperature and heat flux profile at the hot gas wall along the horizontal side (z axis) for a constant (solid line) and variable (dashed line) heat flux profile at evaluation time.

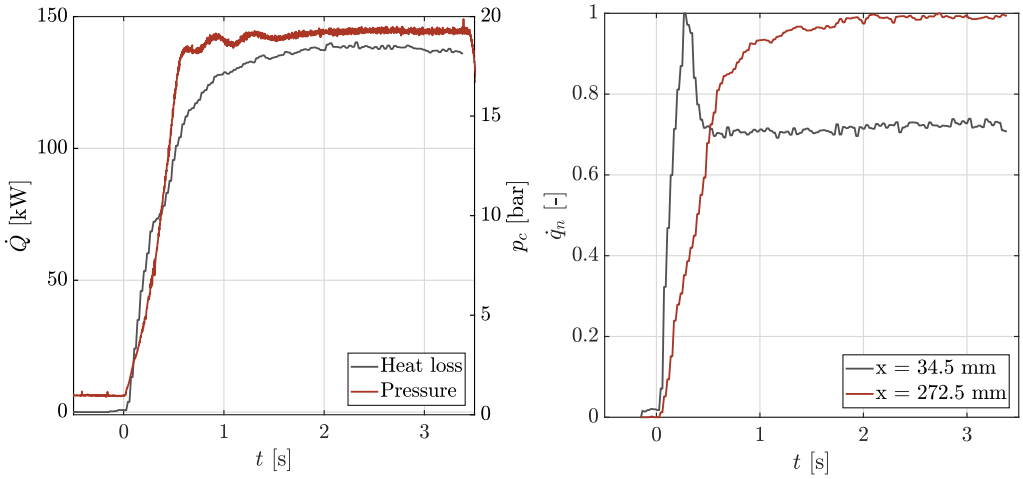

Fig. 19. Time-dependent profile of pressure and heat loss (left) and transient heat flux profiles at selected axial positions (right).

damped away, the energy release in the chamber continues to increase along with the pressure signal and reaches a constant plateau around the $t = 1.5$ s mark. Looking at the pressure signal, one notices that the pressure demonstrates a small oscillation from $t = 0.6$ s until $t = 1.5$ s. The cause of this transient phenomenon could be that the anchoring of the flame in all five injector elements does not happen simultaneously. The elements close to the igniter source are the ones being stabilized faster and the flame propagates to the others slightly later. When the flame is attached and stable, then a constant pressure level is expected. This is also the case at $t = 1.5$ s, which coincides with the time point at which the heat load gets to a plateau as well. Hence the inverse method is able to capture the qualitative transient development of the heat loss through the wall, which is verified by the pressure signal.

Apart from the time evolution of the integrated heat flux over the chamber area, examining the heat flux profile over time at specific locations in the chamber also gives information about the combustion characteristics. In the right sub-figure of Fig. 19, the temporal profile of the heat flux at the 3C location for two different axial planes ($x = 34.5$ mm and $x = 272.5$ mm) is plotted. The heat flux values have been normalized with their respective maximal value in order to emphasize the qualitative effect of the time evolution without taking into account the effect of the difference in absolute value. The values at $x = 34.5$ mm demonstrate a peak after around 0.25 s before reaching a constant level. As explained earlier, this is the effect of the igniter which is located at the same axial position. The results further downstream right before the nozzle segment ($x = 272.5$ mm) seem to be uninfluenced from the igniter effect, since there is no peak present along time. This behavior is expected since start-up effects should be located close to the ignition source and should have disappeared before reaching the end of the combustion chamber.

Therefore it is evident that the inverse method can distinguish between the transient and spatially varying heat loads and the resulting profiles appear to be in agreement with the expected behavior due to the hardware configuration and test sequence.

The main difference between an inverse method used for the heat flux evaluation in a multi-element chamber compared to a single element one is the azimuthal variation of the heat flux profile. In the case of a rectangular combustor as in this case, the variation occurs along the z axis. In order to examine the capability of the method to predict the heat flux variation along the horizontal hot gas wall, the temperature profiles at 1 mm distance from the wall for some selected axial positions and the corresponding heat flux values are examined in Fig. 20.

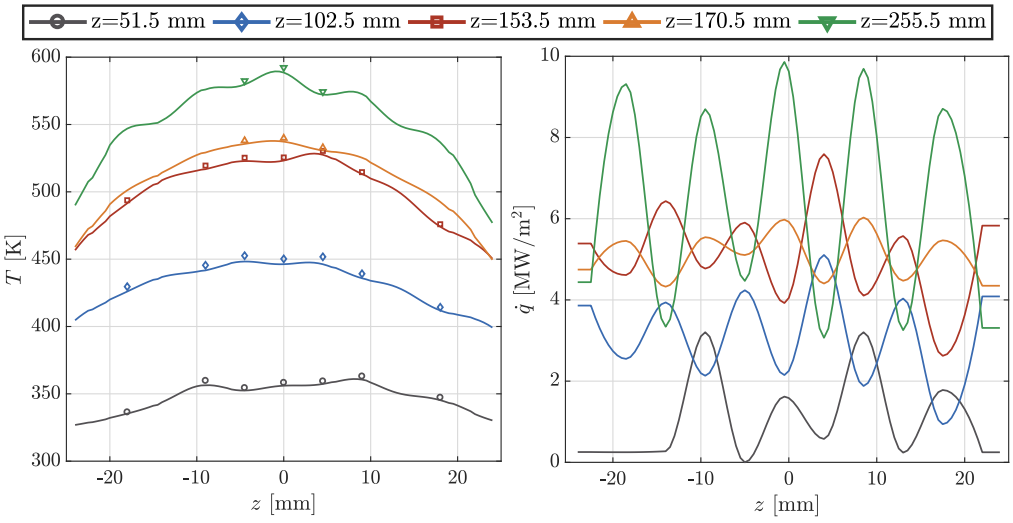

Fig. 20. Temperature at 1 mm from the hot gas wall (left) and heat flux profile at the hot gas wall along the horizontal side (z axis) at evaluation time.

In Fig. 20, the measured values are indicated with symbols and the solid line represents the calculated values stemming from the inverse method. The results are shown at the defined evaluation time window (t = 2-2.5 s). The planes at $x = 51.5$ mm, $x = 102.5$ mm and $x = 153.5$ mm are equipped with all seven thermocouples, whereas at $x = 170.5$ mm and $x = 255.5$ mm only the 3L, 3C and 3R positions are filled. Starting with the plane closest to the faceplate ($x = 51.5$ mm) one notices that the temperature values directly above the injector elements (2C, 3C and 4C) are higher than the measurements between the injectors (3L, 3R). This is also captured in the heat flux profile for the same plane, which demonstrates peaks at the positions 1C, 2C, 3C, 4C and 5C and lower values at the locations in between. This effect of temperature stratification and specifically of higher heat release directly above the elements is expected close to the faceplate where the individual streams have not been mixed and the flow-field can be imagined as five separate cylindrical flames.

The same pattern of maximal heat flux values at the "C" locations is observed at the planes $x = 170.5$ mm and $x = 255.5$ mm as shown in Fig. 20. However, planes $x = 102.5$ mm and $x = 153.5$ mm show the exact opposite effect, with the heat flux values between the injectors being higher than directly above the elements. This results can be deduced by simply looking at the 3L, 3C and 3R temperature measurements for these planes. The effect of the shift in the maximal heat flux azimuthal position has been observed in other sub-scale engines as well. CFD simulations preformed on various engines such as the TUM 7-element sub-scale combustor [23] showed that downstream of a specific location at the chamber, the heat flux values above the injector elements were lower than the ones between two elements of the outer row. This effect was attributed to the presence of strong secondary vortices pushing hot gas out of the injector plane. It is assumed that a similar process takes place in the case of the TUM rectangular combustor.

For positions further downstream than this "shifted" peak, it is expected that the heat flux should be smoother along the z direction, with fewer variations between the maximal and minimal values due to an increase in mixing, leading to a smaller stratification degree. This is indeed observed at the $x = 170.5$ mm where the differences between the heat flux values remain underneath 1 MW/m^2. This is also depicted in the temperature profile which almost has the form of a parabola, with very small variations. In general, observing the trend for all four planes up to the $x = 170.5$ mm location, one sees that the stratification decreases indicating a better mixing of the hot gas.

However the plane at $x = 255.5$ mm demonstrates a further increase in stratification, larger variations of the thermocouple readings and hence obtained heat flux values. Since this would correspond to a decrease in the mixing degree of the burnt gas compared to positions further upstream, the results have to be treated with caution. A possible explanation for this behavior could be a problem with the installation of the thermocouples. If the thermal contact between sensor and chamber material is not adequate then a bigger response time and hence slower measurement can be expected. This could be the case for the 3L and 3R sensors in this plane. Also the sensitivity of the thermocouples' distances from the hot gas wall is also an issue. If the position deviates from the nominal 1 mm, then due to a high sensitivity of the calculated heat flux on the measurement, a bigger heat flux error has to be accounted for. Nevertheless, some flow-dynamic effects could also influence the heat release in this part due to the presence of the truncated nozzle. Due to the sharp edge and the presence of more chamber material at this location, a more detailed CFD analysis is required to fully understand the dynamics of heat release close to the end of combustion. Therefore CFD simulations are also planned to examine whether this effect could be physically possible or if it is a byproduct of the hardware installation.

The high sensitivity of the thermocouple position on the obtained heat flux profile can be grasped by examining Fig. 21. Here the temperature field at the last axial plane before the nozzle is plotted at the evaluation time. The isolines close to the hot gas wall (within the first 2–3 mm) show a "wavy" pattern indicating the variation of the heat flux along the axial position. For distances farther away however, the temperature variation seems to vanish and the isolines show a nearly elliptical form. This implies that positioning the thermocouples in a smallest possible distance from

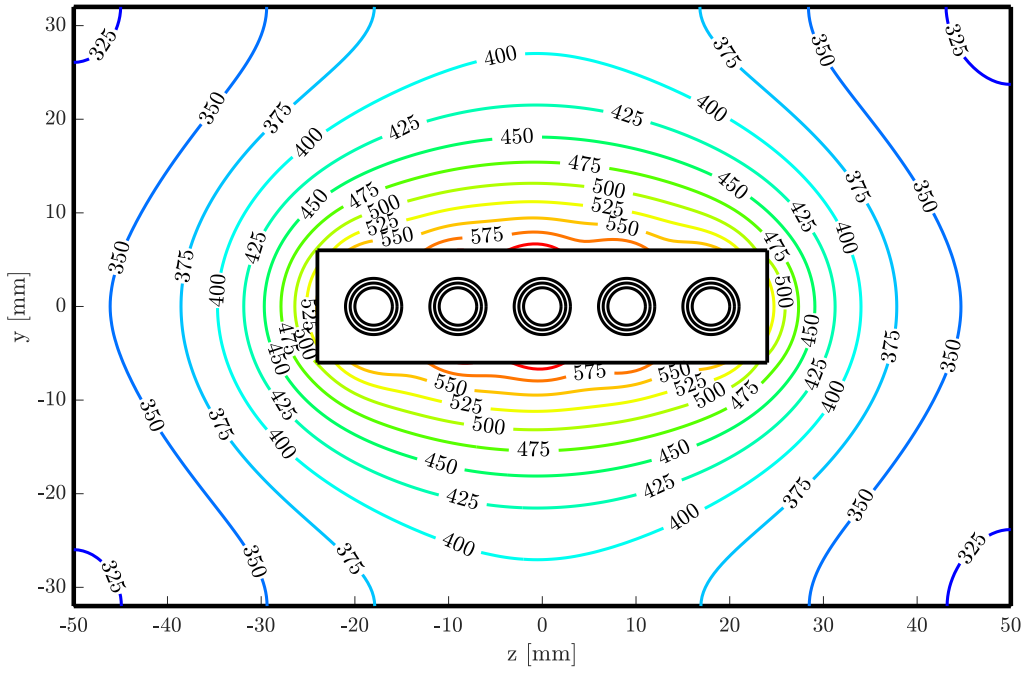

Fig. 21. Temperature field at the plane 272.5 mm downstream of the injector at evaluation time.

the chamber wall is needed for accurate heat flux evaluation. This also implies that a small deviation of the thermocouple from the nominal position or a faulty thermal contact would produce a large heat flux uncertainty because of the high sensitivity.

7. Conclusion

The evaluation of heat flux profiles in single-element and sub-scale engines is crucial for the understanding of the underlying physical and chemical processes defining the injector performance, the injector/injector and injector/wall interaction, mixing and energy release in the chamber. The inverse heat conduction method implemented in RoqFITT is intended for the analysis of transient temperature and heat flux distributions in capacitively cooled rocket thrust chambers and was developed at the Chair of Turbomachinery and Flight Propulsion of the Technical University of Munich.

The inverse method relies on an iterative optimization method with the objective of minimizing the temperature difference between the measured and the calculated values. The optimization variable is the heat flux at discrete locations at the hot gas wall of the chamber. The iterative process requires an efficient direct thermal solver, which has been developed using a finite difference approach on a simplified computational domain. The update of the heat flux parameters at each iteration is carried out using the Jacobi matrix either via the conjugate gradient or the Newton-Raphson method, with the latter one showing a higher computational efficiency. Extensive validation studies of the direct solver and the inverse algorithm have been carried out for operating conditions in a range relevant for sub-scale engine tests.

The inverse heat conduction method has been applied on three capacitively cooled combustors operated at the TUM. Using the algorithm for the evaluation procedure of the tests, important information was extracted from the obtained heat flux profiles regarding the performance of the injector. The qualitative difference in the mixing and energy release process of H_2/O_2 and CH_4/O_2 was captured based on the heat flux profile gradient, allowing for information about the performance characteristics of each propellant combination. The effects of pressure and mixture ratio variations onto the mixing and combustion were also deduced based on the heat flux footprint at the hot gas wall. Moreover, transient effects due to the igniter's operation were identified and validated based on the measured pressure signal. Finally, the heat flux profile along the spanwise direction in a multi-element chamber could also be calculated, showing that the resulting distribution is highly sensitive to measurement noise and systematic errors due to the high thermal conductivity of the structure material.

It has been shown that the inverse heat conduction method can be successfully applied to numerous rocket engine applications for the estimation of the heat loads with reasonable computational resources. Both steady state as well as transient effects can be captured by the use of the method, rendering it a necessary tool for the evaluation of sub-scale experiments.

Conflict of interest

Declarations of interest: none.

Acknowledgements

The authors would like to thank Mr. Cosimo Ciraci and Mr. Alessandro Villani for their assistance in the validation of the code as well as Ms. Simona Silvestri, Ms. Maria Palma Celano and Ms. Fernanda Winter for providing the experimental data. Financial support has been provided by the German Research Foundation (Deutsche Forschungsgemeinschaft DFG) in the framework of the Sonderforschungsbereich Transregio 40.

References

[1] H. Asakawa, H. Nanri, K. Aoki, I. Kubota, H. Mori, Y. Ishikawa, K. Kimoto, S. Ishihara, S. Ishizaki, The status of the research and development of LNG rocket engines in Japan, in: Chemical Rocket Propulsion, Springer, 2017, pp. 463–487.
[2] T. Kato, D. Terakado, H. Nanri, T. Morito, I. Masuda, H. Asakawa, H. Sakaguchi, Y. Ishikawa, T. Inoue, S. Ishihara, et al., Subscale firing test for regenerative cooling LOx/methane rocket engine, in: 7th European Conference for Aeronautics and Space Sciences (EUCASS), 2017. https://doi.org/10.13009/EUCASS2017-381.
[3] O. Knab, M. Frey, J. Görgen, K. Quering, D. Wiedmann, C. Mäding, Progress in combustion and heat transfer modelling in rocket thrust chamber applied engineering, in: 45th AIAA/ASME/SAE/ASEE Joint Propulsion Conference & Exhibit, 2009, p. 5477.
[4] O.J. Haidn, N. Adams, R. Radespiel, W. Schröder, C. Stemmer, T. Sattelmayer, B. Weigand, Fundamental Technologies for the development of future space transport system components under high thermal and mechanical loads, in: 54th AIAA/SAE/ASEE Joint Propulsion Conference, 2018, p. 4466.
[5] F. Cuoco, B. Yang, M. Oschwald, Experimental investigation of LOX/H2 and LOX/CH4 sprays and flames, in: 24th International Symposium on Space Technology and Science, 2004.
[6] J. Lux, D. Suslov, M. Bechle, M. Oschwald, O.J. Haidn, Investigation of sub-and supercritical LOX/methane injection using optical diagnostics, in: 42nd AIAA/ASME/SAE/ASEE Joint Propulsion Conference & Exhibit.
[7] M. Shim, K. Noh, W. Yoon, Flame structure of methane/oxygen shear coaxial jet with velocity ratio using high-speed imaging and OH*, CH* chemiluminescence, Acta Astronaut. 147 (2018) 127–132.
[8] F. Grisch, E. Bertseva, M. Habiballah, E. Jourdanneau, F. Chaussard, R. Saint-Loup, T. Gabard, H. Berger, CARS spectroscopy of CH_4 for implication of temperature measurements in supercritical LOX/CH_4 combustion, Aerosp. Sci. Technol. 11 (1) (2007) 48–54.
[9] D. Suslov, B. Betti, T. Aichner, S. Soller, F. Nasuti, O. Haidn, Experimental investigation and CFD-simulation of the film cooling in an O_2/CH_4 subscale combustion chamber, in: Space Propulsion Conference, 2012.
[10] F. Grisch, P. Bouchardy, W. Clauss, CARS thermometry in high pressure rocket combustors, Aerosp. Sci. Technol. 7 (4) (2003) 317–330.
[11] C.-H. Huang, S.-P. Wang, A three-dimensional inverse heat conduction problem in estimating surface heat flux by conjugate gradient method, Int. J. Heat Mass Transf. 42 (18) (1999) 3387–3403.
[12] C.-H. Huang, Y.-L. Tsai, A transient 3-D inverse problem in imaging the time-dependent local heat transfer coefficients for plate fin, Appl. Therm. Eng. 25 (14–15) (2005) 2478–2495.
[13] E.B. Coy, Measurement of transient heat flux and surface temperature using embedded temperature sensors, J. Thermophys. Heat Transf. 24 (1) (2010) 77–84.
[14] A. Vaidyanathan, J. Gustavsson, C. Segal, One-and three-dimensional wall heat flux calculations in a O_2/H_2 system, J. Propul. Power 26 (1) (2010) 186–189.
[15] M.P. Celano, S. Silvestri, J. Pauw, N. Perakis, F. Schily, D. Suslov, O.J. Haidn, Heat flux evaluation methods for a single element heat-sink chamber, in: 6th European Conference for Aeronautics and Space Sciences (EUCASS), 2015.
[16] N. Perakis, M.P. Celano, O.J. Haidn, Heat flux and temperature evaluation in a rectangular multi-element GOX/GCH4 combustion chamber using an inverse heat conduction method, in: 7th European Conference for Aeronautics and Space Sciences (EUCASS), 2017.
[17] C.U. Kirchberger, Investigation on heat transfer in small hydrocarbon rocket combustion chambers (Ph.D. thesis), Technische Universität München, 2014.
[18] E. Artioukhine, Heat transfer and inverse analysis, in Educational Notes RDP, NATO Unclassified, https://doi.org/10.14339/RTO-EN-AVT-117.
[19] M.N. Özisik, Inverse Heat Transfer: Fundamentals and Applications, CRC Press, 2000.
[20] R. Fletcher, C.M. Reeves, Function minimization by conjugate gradients, Comput. J. 7 (2) (1964) 149–154.
[21] R. Fletcher, Practical Methods of Optimization, John Wiley & Sons, 2013.
[22] C.M. Roth, O.J. Haidn, A. Chemnitz, T. Sattelmayer, G. Frank, H. Müller, J. Zips, R. Keller, P.M. Gerlinger, D. Maestro, et al., Numerical investigation of flow and combustion in a single element GCH4/GOx rocket combustor, in: 52nd AIAA/SAE/ASEE Joint Propulsion Conference, 2016, p. 4995.
[23] N. Perakis, D. Rahn, D. Eiringhaus, Y. Daimon, S. Zhang, S. Karl, T. Horchler, O.J. Haidn, Qualitative and quantitative comparison of RANS simulation results for a 7 element GOX/GCH4 rocket combustor, in: 54th AIAA/SAE/ASEE Joint Propulsion Conference, 2018.
[24] S. Silvestri, F. Winter, M. Garulli, M.P. Celano, G. Schlieben, O.J. Haidn, O. Knab, Investigation on recess variation of a shear coaxial injector in a GOX-GCH4 rectangular combustion chamber with optical access, in: 7th European Conference for Aeronautics and Space Sciences (EUCASS), 2017.
[25] S. Silvestri, C. Kirchberger, G. Schlieben, M.P. Celano, O.J. Haidn, Experimental and numerical investigation of a multi-injector GOX-GCH4 combustion chamber, Trans. Jpn. Soc. Aeronaut. Space Sci. Aerosp. Technol. Jpn. 16 (5) (2018) 374–381.
[26] M.P. Celano, S. Silvestri, C. Bauer, N. Perakis, G. Schlieben, O.J. Haidn, Comparison of single and multi-injector GOX/CH_4 combustion chambers, in: 52nd AIAA/SAE/ASEE Joint Propulsion Conference, 2016, p. 4990.

[27] S. Silvestri, M.P. Celano, G. Schlieben, O.J. Haidn, Characterization of a multi-injector GOX/CH_4 combustion chamber, in: 52nd AIAA/SAE/ASEE Joint Propulsion Conference, 2016, p. 4992.
[28] J. Taylor, Introduction to error analysis, the study of uncertainties in physical measurements, University Science Books, New York, 1997.
[29] X. Wang, Y. Gao, G. Cai, H. Huo, Wall heat transfer measurements in high-pressure combustion devices, J. Aerosp. Eng. 26 (4) (2011) 698–707.
[30] Fluent, 18.0 ANSYS Fluent Theory Guide 18.0, Ansys Inc.
[31] C. Roth, S. Silvestri, N. Perakis, O.J. Haidn, Experimental and numerical investigation of flow and combustion in a single element rocket combustor using GH2/GOX and GCH4/GOX as propellants, in: International Symposium on Space Technology and Science, 2017.
[32] D.R. Bartz, A simple equation for rapid estimation of rocket nozzle convective heat transfer coefficients, J. Jet Propulsion 27 (1) (1957) 49–53.
[33] P. Pempie, Moteur fusees a ergols liquides, Tech. rep., CNES/DLA/AET/A 331/00, 2000.
[34] F.F. Winter, N. Perakis, O.J. Haidn, Emission imaging and CFD simulation of a coaxial single-element GOX/GCH4 rocket combustor, in: 54th AIAA/SAE/ASEE Joint Propulsion Conference, 2018, p. 4764.